Available online at www.sciencedirect.com

ScienceDirect

journal homepage: www.elsevier.com/locate/bbe

Original Research Article

A two dimensional approach for modelling of pennate muscle behaviour

Wiktoria Wojnicz [a,*], Bartlomiej Zagrodny [b], Michal Ludwicki [b], Jan Awrejcewicz [b], Edmund Wittbrodt [a]

[a] Gdansk University of Technology, Gdansk, Poland
[b] Lodz University of Technology, Lodz, Poland

ARTICLE INFO

Article history:
Received 23 August 2016
Accepted 22 December 2016
Available online 24 February 2017

Keywords:
Muscle
Pennation
Rheology
Modelling
Numerical Simulation

ABSTRACT

The purpose of this study was to elaborate a two-dimensional approach for unipennate and bipennate striated skeletal muscle modelling. Behavior of chosen flat pennate muscle is modelled as a rheological system composed of serially linked passive and active fragments having different mechanical properties. Each fragment is composed of three elements: mass element, elastic element and viscous element. Each active fragment furthermore contains the contractile element. Proposed approach takes into consideration that muscle force depends on a planar arrangement of muscle fibers. Paper presents results of numerical simulations, conclusions deduced on the base of these results and a concept of experimental verification of proposed models.

1. Introduction

The human movement system consists of striated skeletal muscles that have different architectures. Among these muscles are fusiform muscles and pennate muscles (unipennate muscles, bipennate muscles and multipennate muscles) [1]. The fusiform muscle fibres run generally parallel to the muscle axis (it is line connecting the origin tendon and the insertion tendon). The unipennate muscle fibres run parallel to each other but at the pennation angle to the muscle axis [2]. The bipennate muscle consists of two unipennate muscles that run in two distinct directions (i.e. different pennation angles). The multipennate muscle is composed of a few bundles of fibres that run in distinct directions.

From the physiology point of view, the unipennate muscle consists of three parts: the muscle insertion (insertion tendon), the belly (muscle fibres), and the muscle origin (origin tendon). It is assumed that during contraction the belly maintains the isovolume, each tendon moves only along its axis and muscle fibres become more pennated, i.e. the pennation angle is increased [3].

The spatial arrangement of pennate muscle fibres determines the muscle fibres length, the lengths of tendons and mechanical properties of muscle. That is why the contractile characteristic (i.e. force-generating capacity) depends on the pennation angle [2]. Moreover, one should take into consideration that a real pennate muscle is a non-homogenous structure: the distal muscle fascicles tend to contract more (i.e.

* *Corresponding author at*: Gdansk University of Technology, ul. G. Narutowicza 11/12, 80-233 Gdansk, Poland.
E-mail address: wiktoria.wojnicz@pg.gda.pl (W. Wojnicz).

http://dx.doi.org/10.1016/j.bbe.2016.12.004

they act at greater pennation angles) than the more proximal muscle fascicles.

Applying an imaging technique, such as nuclear magnetic resonance (MRI) or ultrasonography (US), with a motion capture technique, one might perform in vivo non-invasive measurements to estimate volumes of muscles, muscle fibres lengths and pennation angles [2]. However, one should perform invasive measurements to obtain [4]: 1) parameters describing mechanical properties of chosen muscles (by applying tensile tests and sonomicrometry); 2) muscle morphology and its architecture evaluated at the microscopic level (by using a muscle biopsy); 3) muscle static characteristic (length-force dependence); 4) muscle dynamic characteristic (velocity–force dependence); 5) muscle-tendon parameters used in the Hill-type muscle model. That is why a very limited amount of data describing mechanical properties of pennation muscles can be found in literature.

To model behaviour of pennate muscle one should take into consideration that spatial arrangement of muscle fibres influence mechanical properties and contractile properties of this muscle. Nowadays, to describe pennate muscle function in muscle biomechanics there are applied rheological models: Hill-type muscle models and Hill-Zajac muscle models [3,5–11]. However, application of these models is very limited due to problems related to the obtainment of model parameters. To deal with these problems an optimization technique (i.e. mathematical optimization) can be applied. However, in this case the problem of compatibility between chosen cost function and an alive muscle physiology should be considered.

The three-dimensional (3D) muscle models that take into consideration spatial muscle fibres arrangement are also proposed [12–18]. To apply chosen 3D muscle model, one needs to define the 3D geometry, interaction between components of this model (e.g. lateral transmission of tension between muscle fibres), boundary conditions and material properties according to the principles of continuum mechanics. The fundamental problem consists in identification of material properties because of constrained range of alive tissue experiments. Moreover, these 3D muscle models are applied for static or quasi-static solutions and are incompatible to solve forward dynamics tasks because these models are computational expenses.

Deliberating an application of high-mentioned Hill-type muscle models, Hill-Zajac muscle models or three-dimensional (3D) muscle models, one should define for each muscle examined: muscle static characteristic, muscle dynamic characteristic, tendon static characteristic, physiological cross section area (PCSA), optimal muscle length and optimal muscle force. Due to limited possibility of an alive muscle examination, these characteristics and parameters are defined by making additional assumptions and presuming that a muscle force can be predicted on the base of the value of PCSA and maximum muscle stress or/and a static characteristic of sarcomere (relationship between a sarcomere length and isometric force of this sarcomere). Moreover, in the case of pennate muscle modelling one should take into consideration that muscle force depends on the spatial arrangement of muscle fibres and that is why above-mentioned characteristics and parameters must be estimated for each pennate muscle in the range of its physiological behaviour.

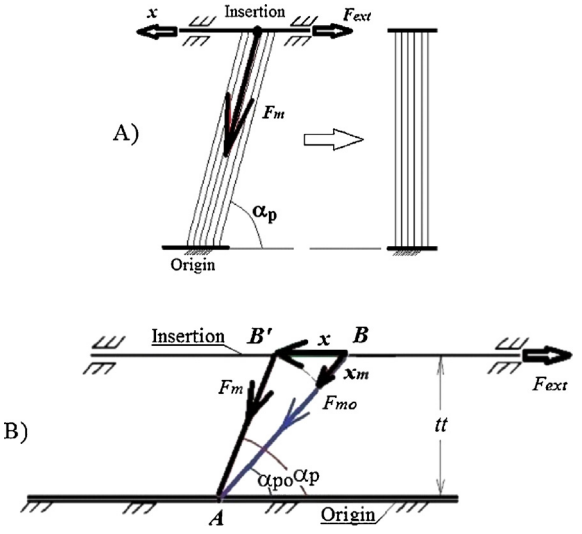

Fig. 1 – Deformation schema of unipennate muscle: A) directions of acting of external force F_{ext} and contractile muscle force F_m towards the muscle insertion displacement x; B) schema of deformation of unipennate muscle (AB – the initial length of muscle (before contraction); AB' – the finish length of muscle (after contraction); F_{mo} – initial contractile muscle force at the length of muscle equals AB; F_m – finish contractile muscle force at the length of muscle equals AB'; α_{po} – the pennation angle before contraction (at the length of muscle equals AB); α_p – the pennation angle after contraction (at the length of muscle equals AB'); x_m – change of muscle length that is equal to the difference of the length AB and the length AB') [19].

To model behaviour of chosen flat pennate muscle one should take into account a planar kinematics, which is described by using at least two parameters (two-dimensional approach). The purpose of this study was to elaborate a two-dimensional approach for unipennate and bipennate striated skeletal muscle modelling by applying a method described in [19]. According to this approach, a behaviour of chosen flat pennate muscle is modelled as a rheological system composed of serially linked passive and active fragments having different mechanical properties. Each fragment is composed of three elements: mass element, elastic element and viscous element. Each active fragment furthermore contains the contractile element. Proposed approach takes into consideration that muscle force depends on a planar arrangement of muscle fibres. The scope of presented study was to perform numerical researches and to elaborate a concept of experimental verification.

2. Method of modelling

2.1. *Principles of pennate muscle modelling*

Assuming a planar deformation schema of unipennate muscle shown in Fig. 1, the mathematical models of unipennate

muscle and bipennate muscle were created. According to this deformation schema, the muscle contraction occurs in the plane (two-dimensional space) along muscle fibres directed at the pennation angle α_p towards the line connecting the muscle insertion (it is a movable part with one degree of freedom) and the muscle origin (it is a non-movable part). It is assumed that during muscle contraction the muscle width tt is constant (according to [20]) and muscle fibres generate a contractile muscle force F_m, which causes the displacement of muscle insertion x and counterbalances an external force F_{ext}:

$$F_{ext} = F_m \cdot \cos\alpha_p \tag{1}$$

During contraction the muscle fibres are shortening and the muscle insertion is translated from the point B to the point B' (the distance BB' is equal to the muscle insertion displacement x). It causes the change of pennation angle: the initial value of pennation angle α_{po} (at the length of muscle equals AB), is changed to the value α_p (at the length of muscle equals AB'). Analyzing the deformation schema of unipennate muscle, the following geometric relation can be derived:

$$tt = AB \cdot \cos\alpha_{po} = AB' \cdot \cos\alpha_p. \tag{2}$$

Taking into consideration a deformation schema of unipennate muscle, five rheological models were created [19]:

1) Unipennate muscle model WW (part 2.2);
2) Unipennate muscle model BZ (part 2.3);
3) Hill-Zajac unipennate muscle model (part 2.4);
4) Bipennate muscle model WW (part 2.5);
5) Bipennate muscle model BZ (part 2.6).

Assuming that the time variable is t, proposed models can be applied to solve the dynamics task formulated in three following problems:

1) Input variables are the muscle insertion displacement $x(t)$ and the external force $F_{ext}(t)$; output variables are the internal force $P^w(t)$ (this force is generated by the contractile elements of muscle model and it causes an appearing of contractile muscle force $F_m(t)$), the pennation angle $\alpha_p(t)$ and deformations of muscle model parts (for chosen muscle models);
2) Input variables are the muscle insertion displacement $x(t)$ and the internal force $P^w(t)$; output variables are the external force $F_{ext}(t)$, the pennation angle $\alpha_p(t)$ and deformations of muscle model parts (for chosen muscle models);
3) Input variables are the external force $F_{ext}(t)$ and the internal force $P^w(t)$; output variables are the muscle insertion displacement $x(t)$, the pennation angle $\alpha_p(t)$ and deformations of muscle model parts (for chosen muscle models).

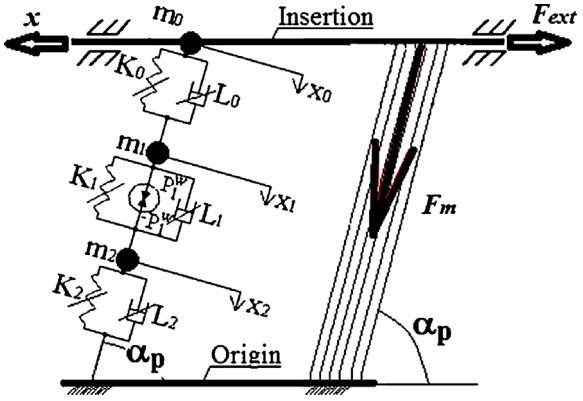

Fig. 2 – Unipennate muscle model WW (rheological model) [19].

2.2. *Unipennate muscle model WW*

The unipennate muscle model WW describes behaviour of unipennate muscle with the pennation angle equals α_p (Fig. 2). This muscle behaviour is described by the rheological model created on the base of the rheological model of fusiform muscle published in [21,22]. The rheological model of unipennate muscle model WW is composed of serially linked three fragments (two passive (non-contractile) fragments and one active (contractile) fragment) that describe different mechanical properties of muscle parts. Each fragment is composed of mass element, elastic element and viscous element. Active fragment has additionally a contractile element that models an ability of muscle to contract. Two lateral fragments model the passive muscle parts (muscle-tendon connections of the muscle insertion and the muscle origin). One middle fragment models the active muscle part (i.e. muscle belly). This model has three degrees of freedom. According to this model: 1) the difference of displacements $(x_0 - x_1)$ describes the length change of upper passive muscle fragment; 2) the difference of displacements $(x_1 - x_2)$ describes the length change of middle active muscle fragment; 3) the displacement x_2 describes the length change of lower passive muscle fragment.

The mathematical model of the unipennate muscle model WW is described by the system of three differential equations:

$$\begin{aligned} &m_0\cdot\ddot{x} + L_0\cdot(\dot{x}_0-\dot{x}_1)\cdot\cos\alpha_p + K_0\cdot(x_0-x_1)\cdot\cos\alpha_p = -F_{ext}(t)\\ &m_1\cdot\ddot{x}_1 + L_0\cdot(\dot{x}_1-\dot{x}_0) + K_0\cdot(x_1-x_0) + L_1\cdot(\dot{x}_1-\dot{x}_2) + K_1\cdot(x_1-x_2) = P_1^w(t)\\ &m_2\cdot\ddot{x}_2 + L_1\cdot(\dot{x}_2-\dot{x}_1) + K_1\cdot(x_2-x_1) + L_2\cdot\dot{x}_2 + K_2\cdot x_2 = -P_1^w(t) \end{aligned} \tag{3}$$

and following geometric relations:

$$\alpha_p = \arcsin\left(\frac{l_0\cdot\sin\alpha_{po}}{l_0-x_0}\right) \tag{4A}$$

$$x_0 = l_0 + \frac{x\cdot\cos\alpha_{po}-l_0}{\cos(\alpha_p-\alpha_{po})} \tag{4B}$$

$$\dot{x}_0 = \frac{dx_0}{dt} = \frac{\dot{x}\cdot\cos\alpha_{po}}{\cos(\alpha_p-\alpha_{po}) - A(x_0)\cdot\sin(\alpha_p-\alpha_{po})\cdot(x_0-l_0)} \tag{4C}$$

$$A(x_0) = \frac{l_0\cdot\sin\alpha_{po}}{(l_0-x_0)^2}\cdot\frac{1}{\sqrt{1-\left(\frac{l_0\cdot\sin\alpha_{po}}{l_0-x_0}\right)^2}} \tag{4D}$$

where m_j is the mass of the j-th element; K_j the stiffness coefficient of the j-th elastic element; L_j the damping coefficient of the j-th viscous element; $P_1^w(t)$ the internal force of the contractile element; l_0 the initial length of muscle model; α_{po} the initial pennation angle when the length of muscle model is equals to its initial length l_0.

2.3. *Unipennate muscle model BZ*

The unipennate muscle model BZ describes behaviour of unipennate muscle with the pennation angle equals α_p (Fig. 3). This model is similar to the unipennate muscle model WW (part 2.2). The unipennate muscle model BZ takes into consideration that stiffness and dumping characteristics of skeletal muscle is described by a nonlinear relationship according to [23,24]:

1) $K_j = k_j \cdot x_j^2$, $j = w$, z, 1,2, where k_j is a correction factor of stiffness;
2) $C_j = c_j \cdot \dot{x}_j^2$, $j = w$, z, 1, 2, where c_j is a correction factor of damping.

Applying the geometric relations (4A-4D), the mathematical model of unipennate muscle model BZ is described by the system of two following equations:

$$\begin{aligned} &m_w \cdot \ddot{x}_w + C_w \cdot \dot{x}_w + K_w \cdot x_w - \frac{C_z \cdot (\dot{x}_z - \dot{x}_1) + K_z \cdot (x_z - x_1)}{\cos\alpha_p} = P_w(t) \\ &m_z \cdot \ddot{x}_z - C_z \cdot (\dot{x}_z - \dot{x}_1) - K_z \cdot (x_z - x_z) = -F_{ext}(t) \end{aligned} \quad (5)$$

where $x_1 = x_w \cdot \cos\alpha_p$; x_w is the displacement of mass m_w; x_z the displacement of mass m_z, $P_w(t)$ the internal force of contractile element.

2.4. *Hill-Zajac upipennate muscle model*

The Hill-Zajac unipennate muscle model describes behaviour of unnipennate muscle by using the Hill-type muscle model and Zajac muscle model (this is a Hill type muscle model, in which the angle of pennation α_p is taken into consideration). There are a lot of modifications of these models [4,25]. In this paper it was assumed that Hill-Zajac unipennate muscle model has a rheological structure shown in Fig. 4. In this model

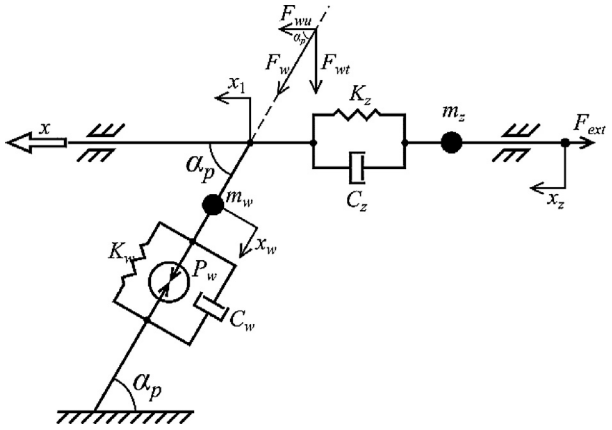

Fig. 3 – Unipennate muscle model BZ [19].

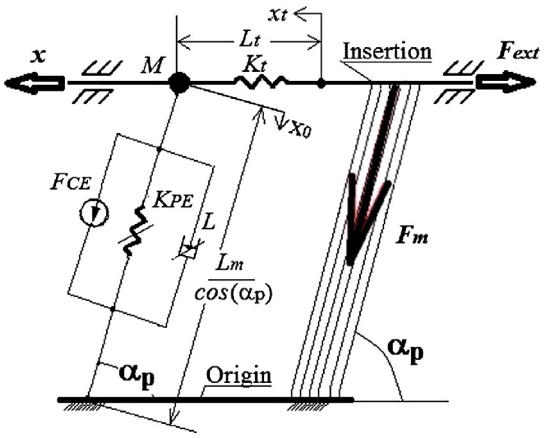

Fig. 4 – Hill-Zajac unipennate muscle model (rheological model) [19].

the muscle length is the sum of belly length $L_m/\cos(\alpha_p)$ and tendon length L_t. Mechanical properties of muscle are described by using a mass element M (this is a muscle mass reduced to a point) and parallel linking of three elements: a contractile element that generates a force F_{CE} (it depends on the actual muscle length l, velocity of muscle fibres contraction and activation Act that originate from a nervous system), a parallel elastic element described by a stiffness coefficient equals K_{PE} and a viscous element described by a damping coefficient equals L. Tendon behaviour is modelled by using an elastic element and its force depends on the tendon stiffness coefficient K_t and the tendon elongation described by a difference of displacements $(x_t - x)$.

The mathematical model of Hill-Zajac unipennate muscle model is described by the system of two equations:

$$\begin{aligned} &F_{ext} + K_t \cdot (x - x_t) = 0 \\ &M \cdot \ddot{x} + K_t \cdot (x - x_t) = F_m \cdot \cos\alpha_p \end{aligned} \quad (6)$$

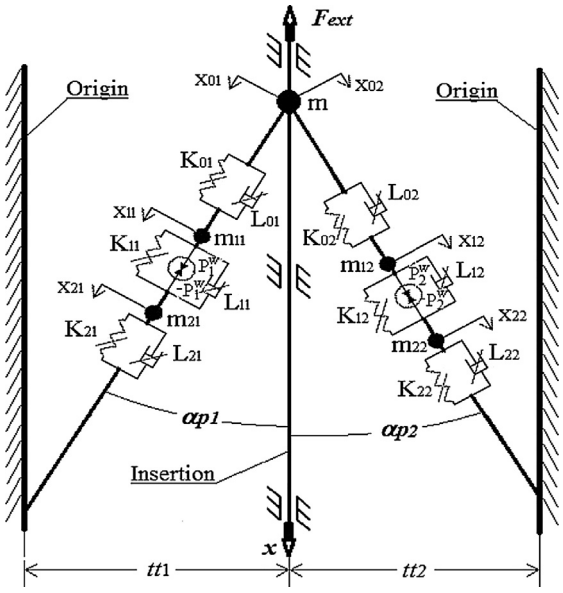

Fig. 5 – Bipennate muscle model WW (rheological model) [19].

where the contractile muscle force is equals to:

$$F_m = F_{CE} - K_{PE}\cdot x_0 - L\cdot \dot{x}_0 \tag{7}$$

It was assumed that force of contractile element F_{CE} depends on the muscle activation *Act*, the muscle length l and difference between the active component of static muscle characteristic F_m^{act} and the passive component of static muscle characteristic F_m^{pas}:

$$F_{CE} = Act\cdot(F_m^{act}(l) - F_m^{pas}(l)) \tag{8}$$

To implement the Hill-Zajac unipennate muscle model there were used: 1) a static muscle characteristic (length-force relationship) proposed in [20]; 2) a static tendon characteristic (elongation-force relationship) proposed in [3]; 3) a dynamic muscle characteristic (velocity-force relationship) published in [3]; 4) data described musculotendon properties (the maximum isometric muscle force, the optimal muscle fibre length, the tendon slack length) according with [20].

2.5. *Bipennate muscle model WW*

The bipennate muscle model WW described behaviour of bipennate muscle composed of two parts directed at the pennation angle α_{p1} (left part with a constant muscle width tt_1) and the pennation angle α_{p2} (right part with a constant muscle width tt_2) towards the muscle insertion (it is movable part) and muscle origins (there are non-movable parts) (Fig. 5). Each muscle part behaviour is modelled as a rheological model of the unipennate muscle WW described in the part 2.2 (i.e. each muscle part is composed of two passive fragments and one active fragment). The bipennate muscle model WW has six degrees of freedom. According to this model: 1) difference of displacements $(x_{01} - x_{11})$ describes the length change of upper passive fragment of muscle left part; 2) difference of displacements $(x_{11} - x_{21})$ describes the length change of middle active fragment of muscle left part; 3) displacement x_{21} describes the length change of lower passive fragment of muscle left part; 4) difference of displacements $(x_{02} - x_{12})$ describes the length change of upper passive fragment of muscle right part; 5) difference of displacements $(x_{12} - x_{22})$ describes the length change of middle active fragment of muscle right part; 6) displacement x_{22} describes the length change of lower passive fragment of muscle right part.

The mathematical model of bipennate muscle model WW is described by the system of five differential equations:

$$\begin{aligned}
&m\cdot\ddot{x} + L_{01}\cdot(\dot{x}_{01}-\dot{x}_{11})\cdot\cos\alpha_{p1} + K_{01}\cdot(x_{01}-x_{11})\cdot\cos\alpha_{p1}\\
&\quad + L_{02}\cdot(\dot{x}_{02}-\dot{x}_{12})\cdot\cos\alpha_{p2} + K_{02}\cdot(x_{02}-x_{12})\cdot\cos\alpha_{p2} = -F_{ext}(t)\\
&m_{11}\cdot\ddot{x}_{11} + L_{01}\cdot(\dot{x}_{11}-\dot{x}_{01}) + K_{01}\cdot(x_{11}-x_{01}) + L_{11}\cdot(\dot{x}_{11}-\dot{x}_{21})\\
&\quad + K_{11}\cdot(x_{11}-x_{21}) = P_1^w(t)\\
&m_{21}\cdot\ddot{x}_{21} + L_{11}\cdot(\dot{x}_{21}-\dot{x}_{11}) + K_{11}\cdot(x_{21}-x_{11}) + L_{21}\cdot\dot{x}_{21} + K_{21}\cdot x_{21} = -P_1^w(t)\\
&m_{12}\cdot\ddot{x}_{12} + L_{02}\cdot(\dot{x}_{12}-\dot{x}_{02}) + K_{02}\cdot(x_{12}-x_{02}) + L_{12}\cdot(\dot{x}_{12}-\dot{x}_{22})\\
&\quad + K_{12}\cdot(x_{12}-x_{22}) = P_2^w(t)\\
&m_{22}\cdot\ddot{x}_{22} + L_{12}\cdot(\dot{x}_{22}-\dot{x}_{12}) + K_{12}\cdot(x_{22}-x_{12}) + L_{22}\cdot\dot{x}_{22} + K_{22}\cdot x_{22} = -P_2^w(t)
\end{aligned} \tag{9}$$

and following geometric relations:

$$\alpha_{p1} = \arcsin\left(\frac{l_{01}\cdot\sin\alpha_{p1}}{l_{01}-x_{01}}\right), \alpha_{p2} = \arcsin\left(\frac{l_{02}\cdot\sin\alpha_{p2}}{l_{02}-x_{02}}\right) \tag{10B}$$

$$\begin{aligned}
\dot{x}_{01} &= \frac{dx_{01}}{dt} = \frac{\dot{x}\cdot\cos\alpha_{p1}}{\cos(\alpha_{p1}-\alpha_{po1}) - A(x_{01})\cdot\sin(\alpha_{p1}-\alpha_{po1})\cdot(x_{01}-l_{01})}\\
\dot{x}_{02} &= \frac{dx_{02}}{dt} = \frac{\dot{x}\cdot\cos\alpha_{p2}}{\cos(\alpha_{p2}-\alpha_{po2}) - A(x_{02})\cdot\sin(\alpha_{p2}-\alpha_{po2})\cdot(x_{02}-l_{02})}
\end{aligned} \tag{10C}$$

$$\begin{aligned}
A(x_{01}) &= \frac{l_{01}\cdot\sin\alpha_{p1}}{(l_{01}-x_{01})^2}\cdot\frac{1}{\sqrt{1-\left(\frac{l_{01}\cdot\sin\alpha_{p1}}{l_{01}-x_{01}}\right)^2}}\\
A(x_{02}) &= \frac{l_{02}\cdot\sin\alpha_{p2}}{(l_{02}-x_{02})^2}\cdot\frac{1}{\sqrt{1-\left(\frac{l_{02}\cdot\sin\alpha_{p2}}{l_{02}-x_{02}}\right)^2}}
\end{aligned} \tag{10D}$$

where m_{ji} is the mass of the j-th element of i-th muscle part; m the mass of the element m_{01} and the element m_{02}; K_{ji} the stiffness coefficient of the j-th elastic element of i-th muscle part; L_{ji} the damping coefficient of the j-th viscous element of i-th muscle part; $P_1^w(t)$ the internal force of the contractile element of left muscle part; $P_2^w(t)$ the internal force of the contractile element of right muscle part; l_{01} the initial length of left part of muscle model; l_{02} the initial length of right part of muscle model; α_{po1} the initial pennation angle when the length of left part of muscle model is equal to l_{01}; α_{po2} the initial pennation angle when the length of right part of muscle model is equal to l_{02}.

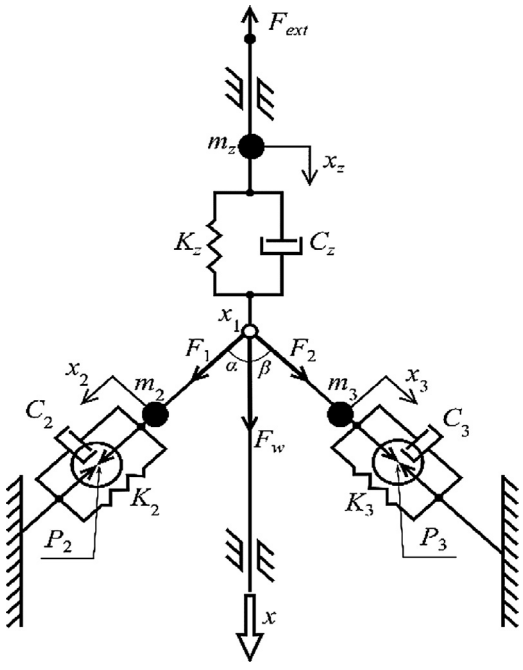

Fig. 6 – Bipennate muscle model BZ [19].

Table 1 – Properties of muscle model (Triceps Brachii Long).

Model	Volume [m^3] [25]	Belly length [m] [25]	Musculotendon length [m] [25]	$\{m_i\}$ [kg] [22,25]	$\{K_i\}$ [N/m] [22]	$\{L_i\}$ [N·s/m] [22]	PCSA [m^2] [25]
Unipennate muscle model WW	0.0002907	0.1524	0.3429	{0.021; 0.307; 0.021}	{5000.0; 937.5; 5000.0}	{500.00; 93.75; 500.00}	[–]
*Unipennate muscle model BZ***	0.0002907	[–]	0.4029	$\{m_z; m_w\}$ = {0.021; 0.307}	$\{K_z; K_w\}$ = {5000; 900}	$\{C_z; C_w\}$ = {1000; 1000}	1.907×10^{-3}
Hill-Zajac unipennate muscle model	0.0002907	0.1524	0.3429	[–]	[–]	[–]	[–]
Bipennate muscle model WW	0.0002907	0.1524	0.3429	{0.021; 0.307; 0.021}	{5000.0; 937.5; 5000.0}	{500.00; 93.75; 500.00}	[–]
*Bipennate muscle model BZ***	0.0002907	[–]	0.4029	$\{m_z; m_2; m_3\}$ = {0.021; 0.307; 0.307}	$\{K_z; K_2\}$ = {5000; 900} ($K_2 = K_3$)	$\{C_z; C_2\}$ = {1000; 1000} ($C_2 = C_3$)	1.907×10^{-3}
$\alpha = \alpha_{p1} = 15^\circ$(left), $\beta = \alpha_{p2} = 15^\circ$ (right)							
*Bipennate muscle model BZ***	0.0002907 (left)	[–]	0.4029 (left)	$\{m_z; m_2; m_3\}$ = {0.021; 0.307; 0.307}	$\{K_z; K_2\}$ = {5000; 900} ($K_2 = K_3$)	$\{C_z; C_2\}$ = {1000; 1000} $C_2 = C_3$	1.907×10^{-3} (left)
$\alpha = \alpha_{p1} = 15^\circ$ (left), $\beta = \alpha_{p2} = 20^\circ$ (right)	0.0002373 (right)		0.2822 (left)				3.845×10^{-3} (left)
*Fusiform muscle model**	0.0002907	0.1524	0.3429	{0.021; 0.307; 0.021}	{5000.0; 937.5; 5000.0}	{500.00; 93.75; 500.00}	[–]

* Unipennate muscle model WW with zero pennate angle.
** Correction factor of stiffness $k_j = 3 \times 10^4$ N/m^3; correction factor of damping $c_j = 3 \times 10^3$ N s^2/m^3.

2.6. *Bipennate muscle model BZ*

The bipennate muscle model BZ described behaviour of bipennate muscle directed at the pennation angle α (left part) and the pennation angle β (right part) towards the muscle insertion (it is movable part) and muscle origins (there are non-movable parts) (Fig. 6).

The bipennate muscle model BZ is similar to the bipennate muscle model WW (part 2.5) but it takes into consideration that stiffness and dumping characteristics of skeletal muscle are nonlinear (part. 2.3). Applying the geometric relationships (10A – 10D), the mathematical model of bipennate muscle model BZ is described by the system of four following equations:

$$\begin{aligned} &m_z\cdot\ddot{x}_z + C_z\cdot(\dot{x}_z - \dot{x}_1) + K_z\cdot(x_z - x_1) = -F_{ext}(t)\\ &m_2\cdot\ddot{x}_2 + C_2\cdot\dot{x}_2 + K_2\cdot x_2 = P_2(t) + F_1(t)\\ &m_3\cdot\ddot{x}_3 + C_3\cdot\dot{x}_3 + K_3\cdot x_3 = P_3(t) + F_2(t)\\ &F_1(t)\cdot\cos\alpha + F_2(t)\cdot\cos\beta = C_z\cdot(\dot{x}_z - \dot{x}_1) + K_z\cdot(x_z - x_1) \end{aligned} \tag{11}$$

where $x_1 = x_2 \cdot \cos\alpha = x_3 \cdot \cos\beta$.

3. Numerical researches

The scope of the paper involved numerical researches of proposed models and elaboration of a concept for further validation of these models. Numerical researches were performed by applying data describing mechanical properties of alive muscles [25]. These researches allowed to obtain muscle behaviour results similar to the published ones [6]. Due to the lack of possibility to examine chosen alive pennate muscle an experimental standing was constructed (p.4). It allowed to perform a comparative quality analysis between a two-dimensional approach proposed to model unipennate and bipennate muscle behaviour and artificial pennate muscle system (p.5).

To perform numerical researches of proposed mathematical models we created their numerical models by applying MATLAB programme and own software created in this programme. To compare behaviours of these models and to prove their physiological correctness the data published in [2,22] were used to simulate a behaviour of unipennate muscle – *long head of triceps brachii muscle* based on the data published [25] (Unipennate muscle model WW, part 2.2; Unipennate muscle model BZ, part 2.3; Hill-Zajac unipennate muscle model, part 2.4). Due to the lack of published data needed to simulate a behaviour of bipennate muscle a hypothetic bipennate muscle was considered: it was formulated as a system composed of two unipennate muscles (*long head of triceps brachii muscle*) (Bipennate muscle model WW, part 2.5; Bipennate muscle model BZ, part 2.6). Detailed properties of examined muscle models are presented in Table 1. Numerical simulations were conducted by applying similar boundary conditions and similar load ($P_1^w(t) = P_2^w(t) = P_w(t) = P_2(t) = P_3(t) = 50\cdot\sigma(t)$ [N], $F_{ext}(t) = 10\cdot\sigma(t)$ [N], where $\sigma(t)$ is the step function). It is worth noting that given load were chosen through series of numerical researches (they provide to obtain physiological changes of muscle fragments lengths).

Numerical model of unipennate muscle model WW (described in part 2.2) was applied to solve three problems

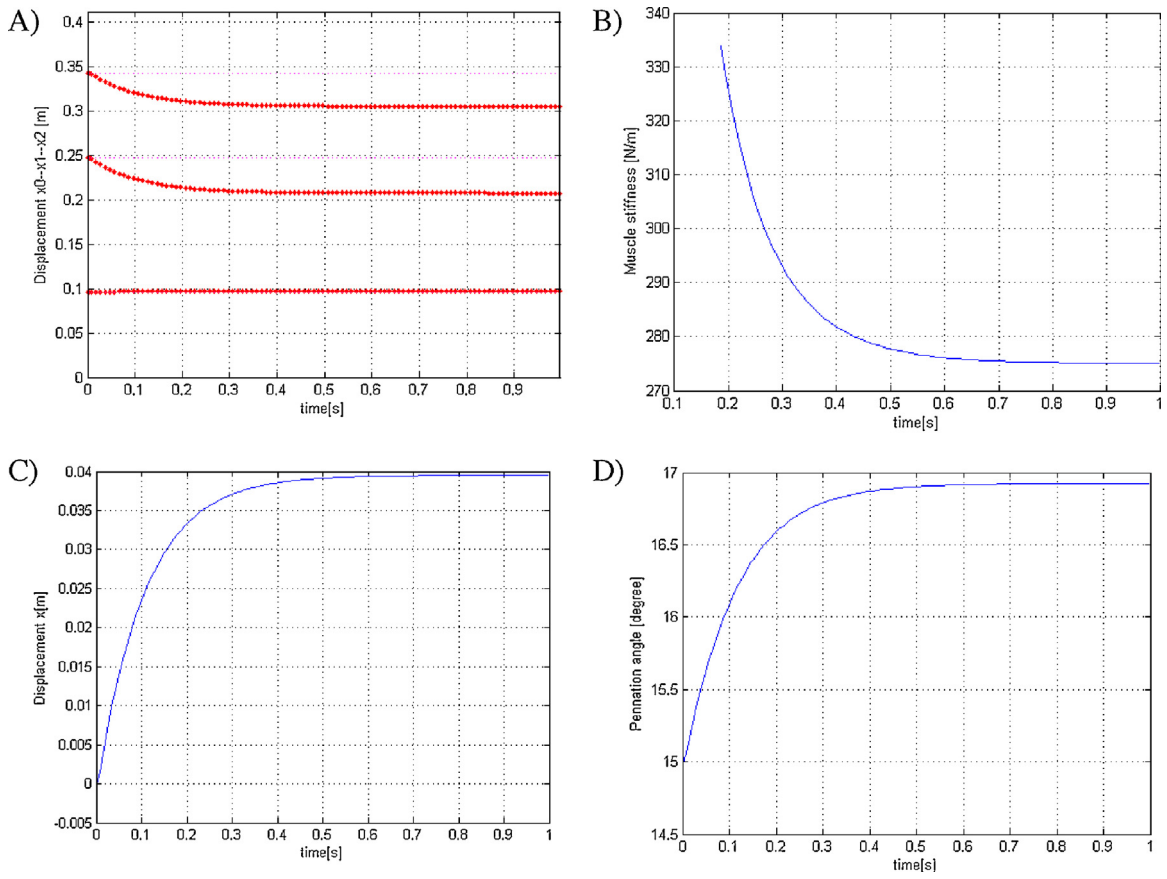

Fig. 7 – Numerical simulation results of unipennate muscle model WW: A) displacement of muscle points; B) stiffness of muscle; C) muscle insertion displacement x; D) pennation angle α_p.

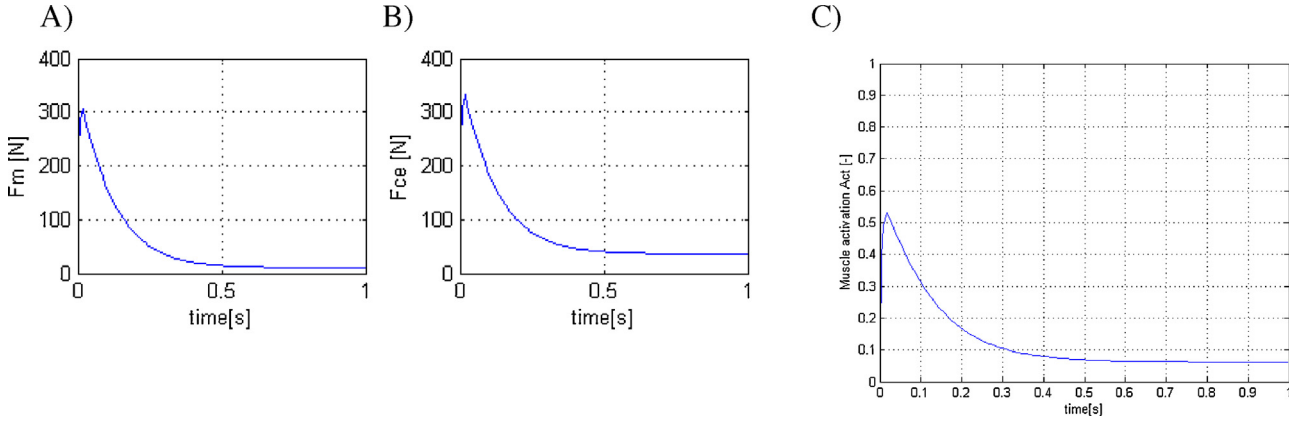

Fig. 8 – Numerical simulation results of Hill-Zajac unipennate muscle model: A) contractile muscle force F_m; B) force of contractile element F_{CE}; C) Muscle activation *Act*.

of the dynamics task described in part 2.1. Fig. 7 shows results obtained from numerical solving of the third problem.

Numerical model of Hill-Zajac unipennate muscle model (described in part 2.4) was applied to solve a dynamics task formulated in the following problem: input variables are the muscle insertion displacement $x(t)$, the pennation angle $\alpha_p(t)$ and the external force $F_{ext}(t)$ (there are numerical simulation results of unipennate muscle model WW); output variables are the contractile muscle force F_m, force of contractile element F_{CE} and muscle activation *Act*. Results obtained from numerical solving of this problem are shown in Fig. 8.

Numerical model of bipennate muscle model WW (described in part 2.5) was applied to solve the third problem of the dynamics task (described in part 2.1). Chosen results obtained from numerical solving of the third problem are shown in Figs. 9 and 10.

Numerical model of unipennate muscle model BZ (described in part 2.3) and bipennate muscle model BZ (described

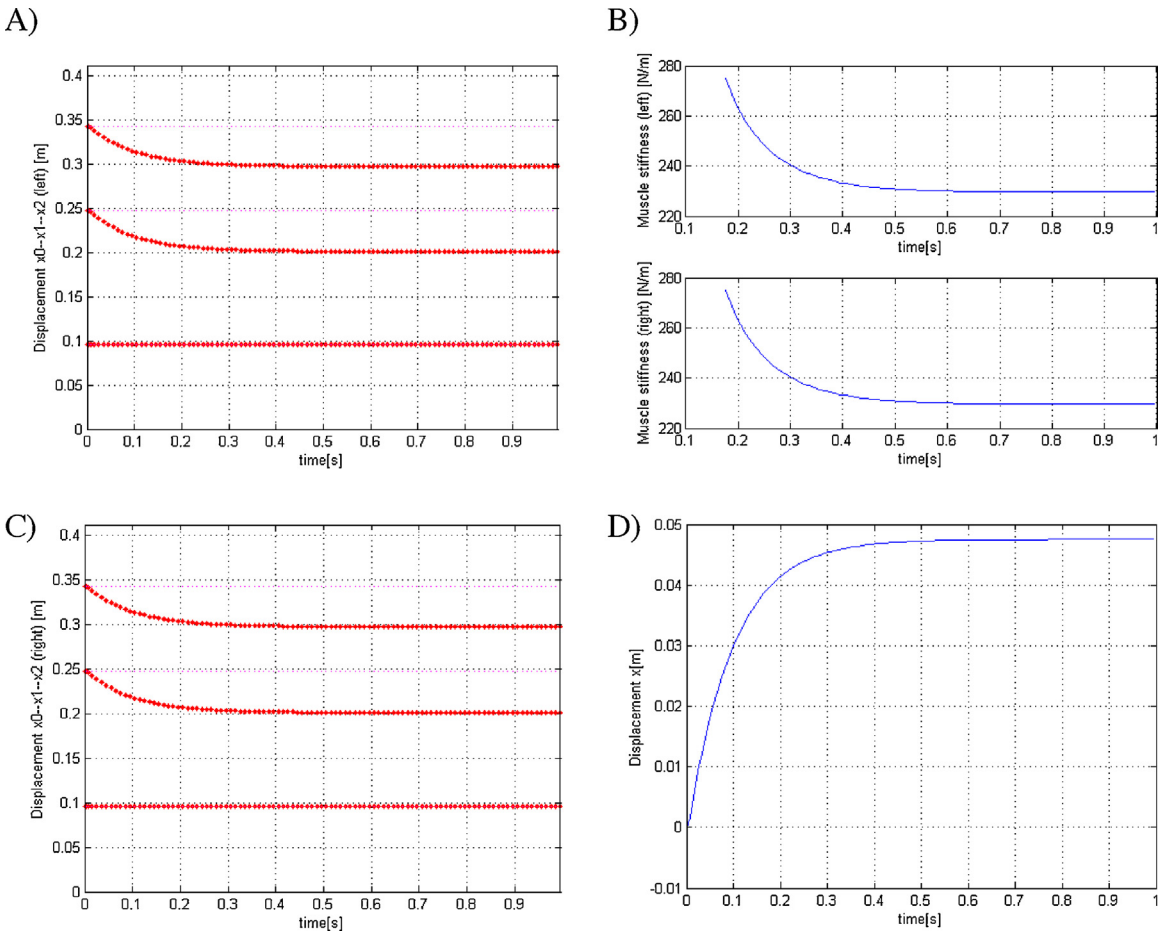

Fig. 9 – Numerical simulation results of bipennate muscle model WW with pennation angles $\alpha_{p1} = \alpha_{p2} = 15^{\circ}$: A) displacement of left muscle part points; B) stiffness of muscle left and right part; C) displacement of right muscle part points; D) muscle insertion displacement x.

in part 2.6) were applied to solve the third problem of the dynamics task (described in part 2.1). Chosen results obtained from numerical solving of the third problem are presented in Figs. 11–13.

To compare the influence of planar arrangement of muscle fibres the numerical model of fusiform muscle model published in [26] was applied to solve the third problem of the dynamics task described in part 2.1. In this case parameters of *long head of triceps brachii muscle* published in [25] were taken into consideration and the angle of pennation was neglected. Fig. 14 shows chosen results obtained from numerical solving of the third problem.

4. Concept of experimental verification

To prove models proposed in this paper a concept of experimental verification was elaborated. According to this concept, a first step consists in applying a non-invasive image analysis and a second step consists in performing experiments by using the prototype of pennate muscle. An image analysis (US or MRI) allows us to perform static image analysis (for a single image) and dynamical image analysis (for a multiple images or a single movie). It is worth noticing that an image analysis requires that an image has high resolution to precisely distinguish muscle fibres [26,27]. Single image of muscle section allows to measure a pennation angle α_p, a muscle diameter d and a muscle length l (Fig. 15). Using specialized image analysis algorithm, like Hough transformation, we created own software, which is able to find average angle of pennation in selected region of medical image. It is worth noting that Hough transformation method is widely used for detecting straight lines in images, e.g. in automatic object orientation or shape recognition [28,29].

The prototype of pennate muscle system was built by using four artificial pneumatic muscles (Fig. 16). Each artificial muscle is a McKibben actuator [30] that can produce the same maximal force, which is independent of the pennation angle. This prototype allows us to form four initial pennation angles: 9°, 14°, 18° and 24°. Experimental normalized static characteristics was obtained, i.e. normalized static force as a function of pennation angle (Fig. 17).

5. Discussion

To analyze results of numerical simulation (researches), three features were taken into consideration: 1) muscle length and

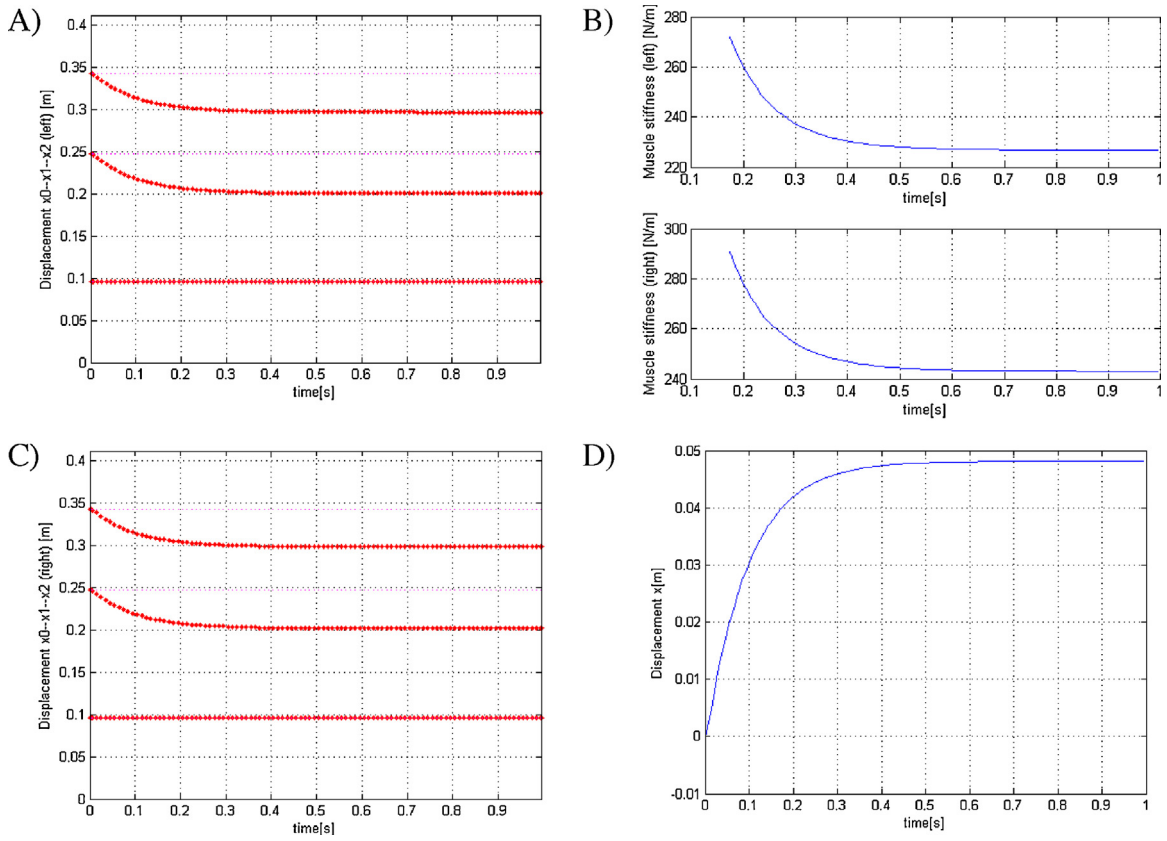

Fig. 10 – Numerical simulation results of bipennate muscle model WW with pennation angles $\alpha_{p1} = 15^\circ$ and $\alpha_{p2} = 20^\circ$: A) displacement of left muscle part points; B) stiffness of muscle left and right part; C) displacement of right muscle part points; D) muscle insertion displacement x.

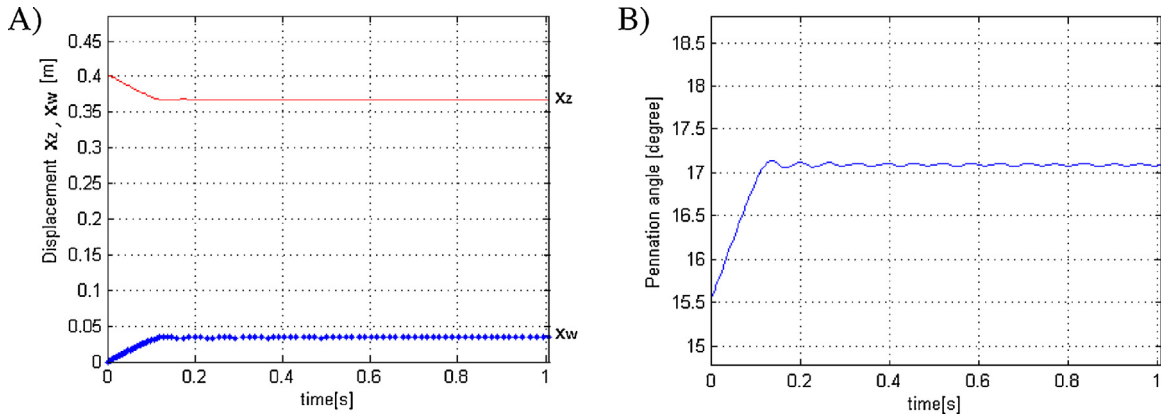

Fig. 11 – Numerical simulation results of unipennate muscle model BZ: A) displacement of the tendon x_z and muscle fibre x_w; B) pennation angle α_p.

pennation angle; 2) muscle stiffness; 3); muscle insertion displacement (Table 2).

Analyzing calculated muscle length and pennation angle, one can infer that: 1) the length change of fusiform muscle model WW are 1.73% more than the length change of unipennate muscle model WW; 2) the length change of left part of bipennate muscle model WW (with $\alpha_{p1} = 15^\circ$ and $\alpha_{p2} = 15^\circ$) are 1.25% less than the length change of left part of bipennate muscle model WW (with $\alpha_{p1} = 15^\circ$ and $\alpha_{p2} = 20^\circ$); 3) the length change of right part of bipennate muscle model WW (with $\alpha_{p1} = 15^\circ$ and $\alpha_{p2} = 15^\circ$) are 1.91% more than the length change of right part of bipennate muscle model WW (with $\alpha_{p1} = 15^\circ$ and $\alpha_{p2} = 20^\circ$); 4) the length change of bipennate muscle model WW (with $\alpha_{p1} = 15^\circ$ and $\alpha_{p2} = 15^\circ$) is 10.53% more than the length change of unipennate muscle model WW; 5) the length change of fusiform muscle model WW are 12.08% more than the length change of unipennate muscle model BZ; 6) the length change of left part of bipennate muscle model BZ (with $\alpha = 15^\circ$ and $\beta = 15^\circ$) are 75.48% more than the length change of left part of bipennate muscle model BZ (with $\alpha = 15^\circ$

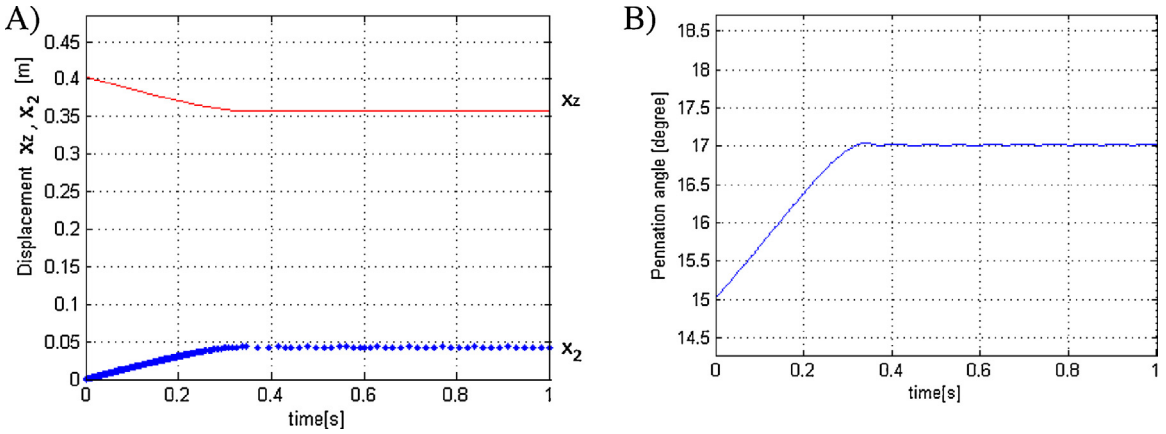

Fig. 12 – Numerical simulation results of bipennate muscle model BZ with pennation angles $\alpha = \beta = 15^{\circ}$: A) displacement of the tendon x_z and muscle fibre $x_2 = x_3$; B) pennation angle $\alpha = \beta$.

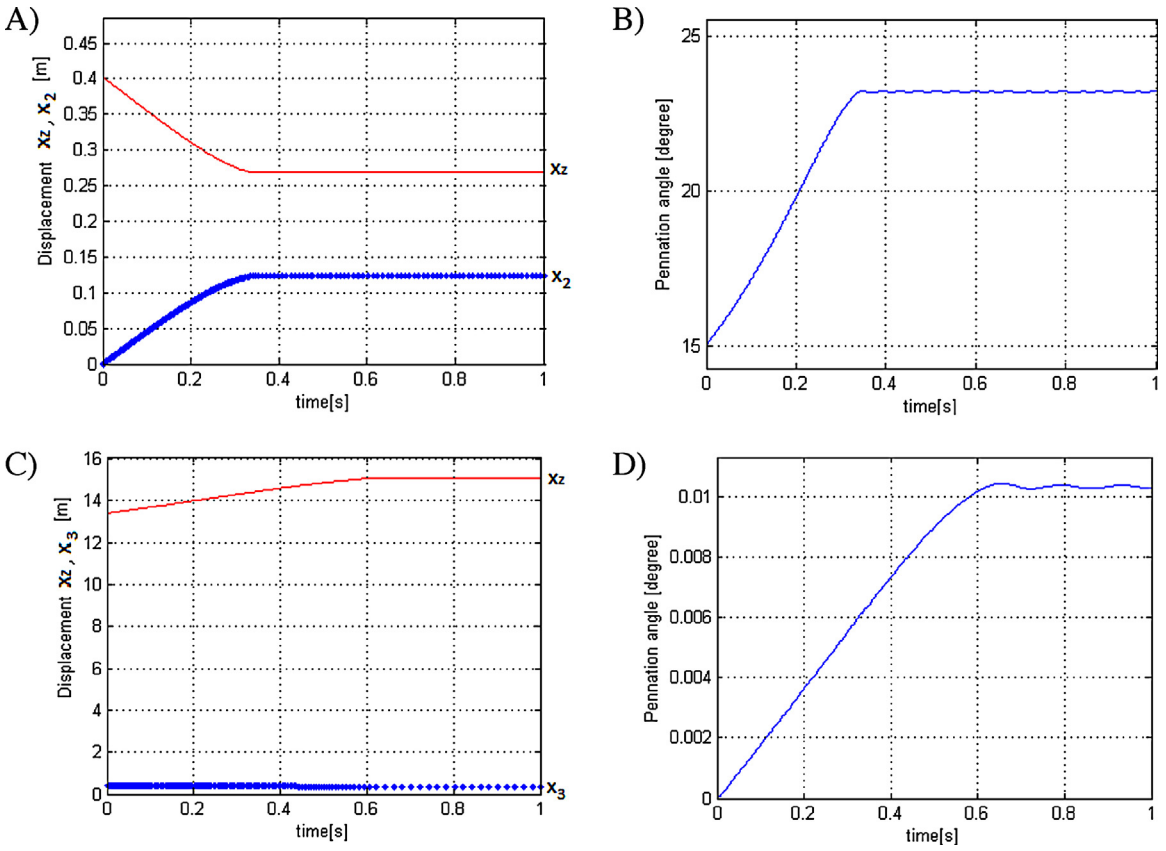

Fig. 13 – Numerical simulation results of bipennate muscle model BZ with pennation angles $\alpha = 15^{\circ}$ (left) and $\beta = 20^{\circ}$ (right): A) displacement of the tendon x_z and muscle fibre x_2; B) pennation angle α; C) displacement of the tendon x_z and muscle fibre x_3; D) pennation angle β.

and $\beta = 20^{\circ}$); 7) the length change of right part of bipennate muscle model BZ (with $\alpha = 15^{\circ}$ and $\beta = 15^{\circ}$) are 9.52% more than the length change of right part of bipennate muscle model BZ (with $\alpha = 15^{\circ}$ and $\beta = 20^{\circ}$); 8) the length change of bipennate muscle model BZ (with $\alpha = 15^{\circ}$ and $\beta = 15^{\circ}$) is 23.53% more than the length change of unipennate muscle model BZ.

Comparing calculated muscle stiffness, one can see that: 1) the stiffness of unipennate muscle model WW is 1.064 times more than stiffness of the fusiform muscle model WW; 2) the stiffness of unipennate muscle model WW is 1,199 times more than the stiffness of bipennate muscle model WW (with $\alpha_{p1} = 15^{\circ}$ and $\alpha_{p2} = 15^{\circ}$); 3) the stiffness of bipennate muscle model WW (with $\alpha_{p1} = 15^{\circ}$ and $\alpha_{p2} = 15^{\circ}$) is more (1,012 for the left and 0,940 times for the right) than the stiffness of bipennate muscle model WW (with $\alpha_{p1} = 15^{\circ}$ and $\alpha_{p2} = 20^{\circ}$); 4) the stiffness of unipennate muscle model BZ is 1,076 times more than stiffness of the fusiform muscle model WW; 5) the stiffness of unipennate muscle model BZ is 1,128 times more

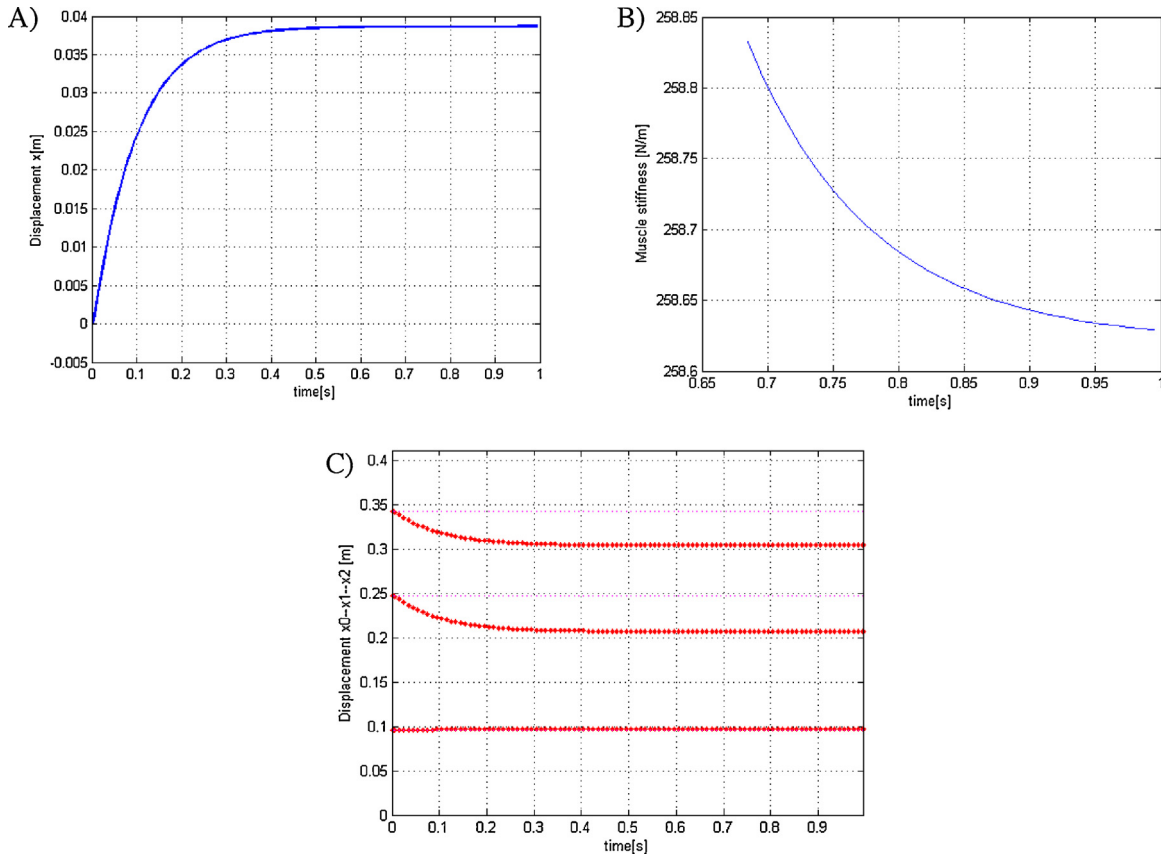

Fig. 14 – Numerical simulation results of fusiform muscle model: A) displacement of muscle insertion $x = x_0$; B) stiffness of muscle; C) displacement of muscle points.

than the stiffness of bipennate muscle model BZ (with $\alpha = 15^\circ$ and $\beta = 15^\circ$); 6) the stiffness of bipennate muscle model BZ (with $\alpha = 15^\circ$ and $\beta = 15^\circ$) is more (3,210 for the left and 0,897 times for the right) than the stiffness of bipennate muscle model BZ (with $\alpha = 15^\circ$ and $\beta = 20^\circ$).

Analyzing muscle insertion displacement, one can see that: 1) muscle insertion displacement of fusiform muscle model WW is 2.20% less than the muscle insertion displacement of unipennate muscle model WW; 2) muscle insertion displacement of unipennate muscle model WW is 22.89% less than the muscle insertion displacement of bipennate muscle model WW (with $\alpha_{p1} = 15^\circ$ and $\alpha_{p2} = 15^\circ$); 3) muscle insertion displacement of bipennate model WW (with $\alpha_{p1} = 15^\circ$ and $\alpha_{p2} = 15^\circ$) is 1.25% less than the muscle insertion displacement of bipennate muscle model WW (with $\alpha_{p1} = 15^\circ$ and $\alpha_{p2} = 20^\circ$); 4) muscle insertion displacement of fusiform muscle model WW is 8.7% more than the muscle insertion displacement of

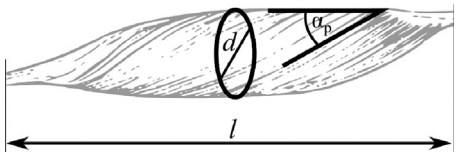

Fig. 15 – Muscle geometrical parameters in visual analysis: pennation angle α_p, muscle diameter d and muscle length l [19].

Fig. 16 – A prototype of pennate muscle (a prototype is composed of four artificial pneumatic muscles) [19].

Table 2 – Numerical examination results calculated for time variable t = 1s.

Model	$\alpha_p(t = 0)$ [°]	$\alpha_p(t = 1s)$ [°]	*Muscle stiffness* (t = 1s) [N/m]	x (t = 1s) $\{x_o\ (t = 1s)\}$ [m]
Unipennate muscle model WW	15.00	16.92	275.1	0.03952 **{0.03800}**
Unipennate muscle model BZ	15.54	17.1	278.2	x_1 = 0.0353 $\{x_w$ = **0.034**}
Hill-Zajac unipennate muscle model	15.00	16.92	275.1	0.03952 **{0.03800}**
Bipennate muscle model WW $\alpha_{p1} = 15^\circ$ (left), $\alpha_{p2} = 15^\circ$ (right)	15.00 (left) 15.00 (right)	17.37 (left) 17.37 (right)	229.5 (left) 229.5 (right)	0.04752 **{0.04565}** (left) 0.04752 **{0.04565}** (right)
Bipennate muscle model WW $\alpha_{p1} = 15^\circ$ (left), $\alpha_{p2} = 20^\circ$ (right)	15.00 (left) 20.00 (right)	17.41 (left) 23.16 (right)	226.7 (left) 243.0 (right)	0.04812 **{0.04622}** (left) 0.04812 **{0.04476}** (right)
Bipennate muscle model BZ $\alpha = \alpha_{p1} = 15^\circ$ (left), $\beta = \alpha_{p2} = 15^\circ$ (right)	15.02 (left) 15.02 (right)	17.01 (left) 17.01 (right)	246.7 (left) 246.7 (right)	x_z = 0.04460 $\{x_2$ = **0.04200**} (left) x_z = 0.04460 $\{x_3$ = **0.04200**} (right)
Bipennate muscle model BZ $\alpha = \alpha_{p1} = 15^\circ$ (left), $\beta = \alpha_{p2} = 20^\circ$ (right)	15.02 (left) 19.99 (right)	23.20 (left) 23.93 (right)	76.9 (left) 275.0 (right)	x_z = 0.04000 $\{x_2$ = **0.01030**}(left) x_z = 0.04000 $\{x_3$ = **0.03800**} (right)
Fusiform muscle model*	[–]	[–]	258.6	0.03867 **{0.03867}**

* Unipennate muscle model WW with zero pennate angle.

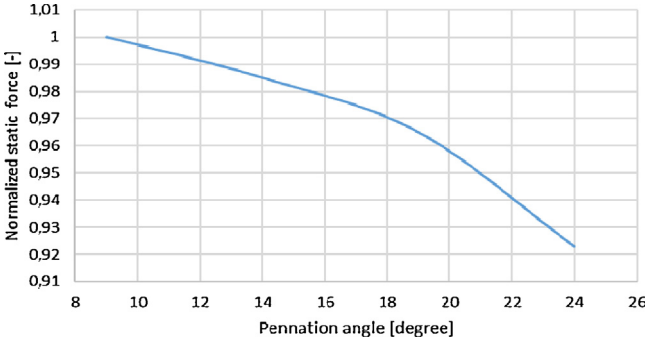

Fig. 17 – Normalized static force as a function of pennation angle [19].

unipennate muscle model BZ; 5) muscle insertion displacement of unipennate muscle model BZ is 26.30% less than the muscle insertion displacement of bipennate muscle model BZ (with $\alpha = 15^\circ$ and $\beta = 15^\circ$); 6) muscle insertion displacement of bipennate model BZ (with $\alpha = 15^\circ$ and $\beta = 15^\circ$) is 10.31% less than the muscle insertion displacement of bipennate muscle model BZ (with $\alpha = 15^\circ$ and $\beta = 20^\circ$).

Analyzing results of Hill-Zajac unipennate muscle model, one can see that calculated muscle force F_m i F_{CE} are bigger than load inputted to each of four proposed rheological models (unipennate muscle model WW, unipennate muscle model BZ, bipennate muscle model WW and bipennate muscle model BZ). Course of calculated muscle activation *Act* is consistent with the nervous system acting, i.e. at the beginning of muscle contraction the activation is a jump function, which is diminished to constant value.

Results presented in Fig. 17 confirms that greater pennation angle causes the diminishment of force measured along a long axis of the muscle (in the case of the same value of muscle force). This behaviour was also confirmed on the base of numerical examination results (p.4).

6. Conclusions

The aim of this study was to create mathematical models of pennate muscle (unipennate muscle and bipennate muscle), perform numerical researches of proposed models and elaborate a concept of experimental verification. Proposed new models (Unipennate muscle model WW, part 2.2; Unipennate muscle model BZ, part 2.3; Bipennate muscle model WW, part 2.5; Bipennate muscle model BZ, part 2.6) were created in the form of rheological models by taking into consideration that muscle contraction occurs in a two-dimension space and the arrangement of muscle fibres influence magnitude of muscle force contraction. According to the proposed approach, a muscle is treated as a complex system composed of different mechanical properties fragments. Each passive fragment is modelled as a mass-viscous-elastic properties structure, thus each active fragment has additionally a contractile element (force producing element). New models can be applied to solve dynamic task by inputting kinematic and/or external/internal force data (p.2.1).

Unipennate muscle model WW and Bipennate muscle model WW can be applied to model a behaviour of pennate muscle having two tendon and one belly. On the other hand, Unipennate muscle model BZ and Bipennate muscle model BZ can be applied to model a non-linear behaviour of pennate

muscle having one tendon and one belly. To perform numerical researches (i.e. to solve chosen system of stiff differential equations) a proper numerical method should be also applied.

In the paper was also considered Hill-Zajac unipennate muscle model (part 2.4), which describes muscle behaviour from the phenomenological point of view (classical approach in biomechanics). Results of this model can be used to comparative study between classical approach and proposed new one.

At this stage of modelling it was assumed that slow and fast muscle fibres have identical mechanical properties. That is why a future study should be performed to detect in what physiological range of pennate muscle functioning proposed approach can be applied.

On the base of numerical simulation results, next conclusions were drawn:

1) efficiency of fusiform muscle (it is a quotient the external force to the contractile muscle force) is more than the efficiency of unipennate muscle (because a unipennate muscle works in a plane and a part of its contractile force is devoted to spatial arrangement of muscle fibres);
2) the efficiency of bipennate muscle is more that the efficiency of unipennate muscle;
3) to model a behaviour of pennate muscle one should precisely describe the geometric relations occurring between pennate muscle fibres (i.e. geometric constrains) and the force-length relations depended on the time variable (i.e. dynamics equations of motion).

Acknowledgments

The work has been supported by the Polish National Science Centre under the grant OPUS 9 No. 2015/17/B/ST8/01700 for years 2016–2018. Calculations were carried out at the Academic Computer Centre in Gdańsk, Poland.

REFERENCES

[1] Nigg BM, Herzog W. Biomechanics of the musculoskeletal system. Chichester: John Wiley & Sons; 1994.
[2] Narici M. Human skeletal muscle architecture studied in vivo by non-invasive imaging techniques: functional significance and applications. J Electromyogr Kinesiol 1999;9:97–103.
[3] Zajac F. Muscle and tendon: properties, models, scaling and application to biomechanics and motor control. Crit Rev Biomed Eng 1989;17:359–410.
[4] Aagaard P, Andersen JL, Poulsen PD, Leffers AM, Wagner A, Magnussin SP, et al. A mechanism for increased contractile strength of human pennate muscle in response to strength training: changes in muscle architecture. J Physiol 2001;534.2:613–23.
[5] Delp SL. Surgery simulation – a computer graphics system to analyze and design musculoskeletal reconstructions of the lower limb. PhD. Thesis. Stanford: Stanford University Press; 1990.
[6] Huijing PA. Muscle, the motor of movement: properties in function, experiment and modeling. J Electromyogr Kinesiol 1998;8:61–77.
[7] McGowan CP, Neptune RR, Herzog W. A phenomenological model and validation of shortening-induced force depression during muscle contractions. J Biomech 2010;43:449–54.
[8] Ambrósio J, Quental C, Pilarczyk B, Folgado J, Monteiro J. Multibody biomechanical models of the upper limb. Procedia IUTAM 2011;2:4–17.
[9] van der Bogert AJ, Blana D, Heinrich D. Implicit methods for efficient musculoskeletal simulation and optimal control. Procedia IUTAM 2011;2:297–316.
[10] McGowan CP, Neptune RR, Herzog W. A phenomenological muscle model to assess history dependent effects in human movement. J Biomech 2013;46:151–7.
[11] Quental C, Folgado J, Abrosio J, Monteiro J. A new shoulder model with a biologically inspired glenohumeral joint. Med Eng Phys 2016;38:969–77.
[12] Yucesoy CA, Koopman BHFJM, Huijing PA, Grootenboer HJ. Three dimensional finite element modeling of skeletal muscle using a two-domain approach: linked fiber-matrix mesh model. J Biomech 2002;35:1253–62.
[13] Lemos RR, Epstein M, Herzog W, Wyvill BA. Framework for structured modeling of skeletal muscle. Comput Methods Biomech Biomed Eng 2004;7(6):305–17.
[14] Blemker SS, Delp SL. Three-dimensional representation of complex muscle architectures and geometries. Ann Biomed Eng 2005;33(5):661–73.
[15] Blemker SS, Pinsky PM, Delp SL. A 3D model of muscle reveals the causes of nonuniform strains in the biceps brachii. J Biomech 2005;38:657–65.
[16] Blemker SS, Delp SL. Rectus femoris and vastus intermedius fiber excursions predicted by three-dimensional muscle models. J Biomech 2006;39:1383–91.
[17] Heidlauf T, Klotz T, Rode C, Altan E, Bleiler C, Siebert T, et al. A multi-scale continuum model of skeletal muscle mechanics predicting force enhancement based on actin-titin interaction. Biomech Model Mechanobiol 2016;1–15.
[18] Virgilio KM, Martin KS, Peirce SM, Blemker SS. Multiscale models of skeletal muscle reveal the complex effects of muscular dystrophy on tissue mechanics and damage susceptibility. Interface Focus 2015;5(20140080):1–10.
[19] Wojnicz W, Zagrodny B, Ludwicki M, Awrejcewicz J, Wittbrodt E. Mathematical model of pennate muscle. Dynamical Systems: Mechatronics and Life Sciences. DSTA 2015 Conference. Lodz: Department of Automation, Biomechanics and Mechatronics. Lodz University of Technology; 2015. p. 595–608.
[20] Garner BA, Pandy MG. Estimation of musculotendon properties in the human upper limb. Ann Biomed Eng 2003;31:207–20.
[21] Wojnicz W, Wittbrodt E. Analysis of muscles' behaviour. Part I. The computational model of muscle. Acta Bioeng Biomech 2009;11:15–21.
[22] Wojnicz W, Wittbrodt E. Application of muscle model to the musculoskeletal modeling. Acta Bioeng Biomech 2012;14:29–39.
[23] Awrejcewicz J, Kudra G, Zagrodny B. Nonlinearity of muscle stiffness. Theor Appl Mech Lett 2012;2(5):1–3.
[24] Soderberg GL, Kinesiology:. Application to pathological motion. Baltimore: Williams & Wilkins; 1986.
[25] Garner BA, Pandy MG. Musculoskeletal model of the upper limb based on the Visible Human Male Dataset. Comput Methods Biomech Biomed Eng 2001;4:93–126.
[26] Noorkoiv M, Stavnsbo A, Aagaard P, Blazevic AJ. In vivo assessment of muscle fascicle length by extended field-of-view ultrasonography. J Appl Physiol 2010;109(6):1974–9.

[27] Csapo R, Malis V, Hodgson J, Sinha S. Age-related greater Achilles tendon compliance is not associated with larger plantar flexor muscle fascicle strains in senior women. J Appl Physiol 2014;116(8):961–9.
[28] Neatpisarnvanit C, Suthakorn J. Intramedullary nail distal hole axis estimation using Blob analysis and Hough transform. Robotics, Automation and Mechatronics, IEEE Conference. 2006. pp. 1–6.
[29] Parsa Y, Hosseinzadeh H, Effatparvar M. Development Hough transform to detect straight lines using pre-processing filter. Int J Inform Security Syst Manage 2015;4 (2):448–56.
[30] Trsagarakis NG, Caldwell DG. Development and control of a ‘‘soft-actuated' exoskeleton for use in physiotherapy and training. Autonomous Robots 2003;15:21–33.